Experimental Investigation of Topology-Optimized Deep Reinforced Concrete Beams with Reduced Concrete Volume

Yan Liu[1], Jackson L. Jewett[1], and Josephine V. Carstensen[1,2]

Massachusetts Institute of Technology, Cambridge MA 02139, USA
jvcar@mit.edu

Abstract. This paper presents an experimental investigation of digitally manufactured, reinforced concrete beams designed with topology optimization. The backbone of the current work is a hybrid mesh topology optimization algorithm that automatically generates strut-and-tie layouts. The resulting designs have tensile truss elements describing the reinforcing phase and compressive continuum force flow elements that illustrates how the concrete is carrying load. The aim of this work is to investigate the effect of removing a percentage of the non-load carrying concrete phase. A beam is designed with a standard, by-hand approach and the same steel amount is used in to generate a topology-optimized design. This work considers three beam designs; (i) the standard, (ii) a topology-optimized beam with a prismatic section (i.e. 100% concrete), and (iii) the topology-optimized steel layout in a beam with a reduced concrete volume (herein 75%). An alternative reinforcement method is used in which steel plates are cut by waterjet. To improve the bond quality between concrete and reinforcement, corrugations and anchors are added to the steel layouts. However, as opposed to previous experimental tests conducted by the authors, a poor bond quality is achieved, leading to premature failures of all test specimens. Due to the lack of proper bonding, comparison can only be made in the early elastic range. Here, a significant trend is that the by-hand and the topology-optimized specimens with 75% concrete exhibit near identical behaviors.

Keywords: Topology optimization · Generative design · Waterjet cut reinforcement · Experimental testing

1 Introduction

With the recent rapid development of digital manufacturing technologies there is a growing need for design methods that fit the new fabrication and construction paradigm. Topology optimization offers a means to leverage the new possibilities since it is free-form generative design approach that does not require the designer to have a preconceived notion of the final layout of the design. It only requires the definition of a design domain with applied loads and boundary conditions, and will seek to efficiently distribute material within this domain. The design problem

is formulated as a formal optimization problem and most rigorously solved using a mathematical program. Topology optimization has been known to lead to new, often complex and surprising solutions that typically outperform conventional low weight designs [1]. Since concrete has an initial liquid, highly formable state, digitally manufactured topology-optimized reinforced concrete (RC) structures have the potential to save material, while maintaining the performance level of conventional designs.

Several topology optimization algorithms have been suggested for improved design of RC structures. Efforts have e.g. focused on automatically designing layouts for strut-and-tie models [2], [3], designing pre-stressed RC [4] or including stress-constraints [5]. However, there exists few literature examples on topology-optimized RC structures that have been built and even fewer examples of experimental testing and validation of the designs. Exceptions include Dombernowsky and Søndergaard [6] that constructed a RC frame designed with a commercial software and Jipa et al. [7] that fabricated two floor slabs of fiber-reinforced ultra-high performance concrete. Recent work by the authors designed, digitally constructed and experimentally tested topology-optimized plain concrete beams [8] and RC beams [9]. In the latter, the reinforcement layout was designed using the bilinear hybrid mesh topology optimization algorithm from Gaynor et al. [3] and test specimens were constructed by waterjet cutting the reinforcement layout from steel plates. These were inserted into prismatic beams. Hand designed beam specimens where thus compared to topology-optimized beams that had the same amounts of both concrete and steel. A 20+% improvement of both stiffness and strength was observed.

This work seeks to design low-weight RC structures that maintain the behavior of conventional RC design. The backbone is an extension of the bilinear hybrid mesh topology optimization algorithm from Gaynor et al. [3]. The algorithm was originally developed to generate strut-and-tie models for deep beams and uses a hybrid truss-continuum mesh. It is set up so that all the force flow in compression is visualized by the continuum elements whereas the tensile forces are guided to the truss elements. The resulting designs provides the steel layouts, ready for sizing, and the beams are intended to be prismatic and have a standard 100% concrete volume. However, the computational design results have regions with zero force flow. This work seeks to experimentally investigate the effects of excluding zero-force regions from the physical designs.

Three deep RC beam designs are experimentally evaluated; (i) a standard design, (ii) a topology-optimized with 100% concrete, and (iii) a topology-optimized design with a reduced concrete volume. All tested beams have the same amount of steel, two will have 100% concrete ((i) and (ii)) and one ((iii)) has a reduced concrete volume. Herein, the reduced concrete volume is chosen to be 75% concrete as it is stipulated that a 25% reduction will not cause problems related to lack of development length.
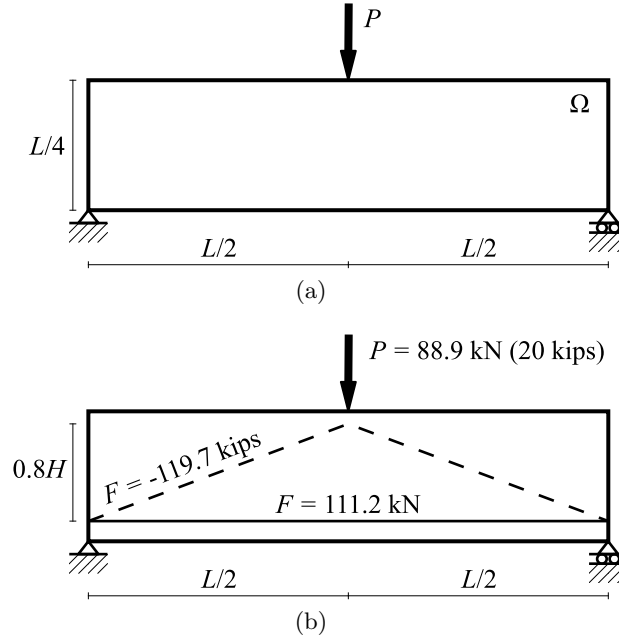
Fig. 1. (a) Simply supported beam design case used herein, and (b) standard strut-and-tie hand calculated design.

1.1 Standard Strut-and-Tie Design

In this work, a simply supported beam design case is considered. The design domain Ω and applied loads and boundary conditions are shown in Fig. 1a. Due to size restrictions of the available testing equipment, the following dimensions are used: $L = 91.4$ cm (36") and $H = 22.9$ cm (9"). The thickness of the beam is taking as $t = 5.1$ cm (2") and the design load is chosen as $P = 88.9$ kN (20 kips).

An initial standard strut-and-tie design is conducted following the ACI 318 [10] guidelines to obtain a control steel volume. A simple strut-and-tie layout is chosen and the forces in all members are found as shown in Fig. 1b. The bottom steel bar is then sized accordingly, resulting in a total steel volume of $V_t = 365.8$ cm^3 (22.32 in^3).

1.2 Topology-Optimized Design

A full review of the original algorithm by Gaynor et al. is beyond the scope of this paper and the reader is referred to [3] for further details. However, in the current work, all beam designs are desired to have the same steel volume. Therefore the topology-optimized design herein is obtained using a slightly modified formulation. The change of formulation ensures that both concrete and steel

volumes can be constrained and is defined as follows:

$$\begin{aligned}
\underset{\boldsymbol{\phi},\ \boldsymbol{\rho}_t}{\text{minimize}} \quad & f(\boldsymbol{\rho}_c, \boldsymbol{\rho}_t, \boldsymbol{\sigma}_c, \boldsymbol{\sigma}_t) = \mathbf{F^T d} \\
\text{subject to} \quad & \mathbf{K}(\boldsymbol{\rho}_c, \boldsymbol{\rho}_t, \boldsymbol{\sigma}_c, \boldsymbol{\sigma}_t)\mathbf{d} - \mathbf{F} = \mathbf{0} \\
& c_c(\boldsymbol{\rho}_c) = \sum_{e \in \Omega_c} \rho_c^e v_c^e - V_c \le 0 \\
& c_t(\boldsymbol{\rho}_t) = \sum_{e \in \Omega_t} \rho_t^e v_t^e - V_t \le 0 \\
& \phi_{min} \le \phi_i \le \phi_{max} \quad \forall\, i \in \Omega_c \\
& 0 \le \rho_t^e \quad \forall\, e \in \Omega_t.
\end{aligned} \tag{1}$$

Here, ϕ_i are the design variables that control the continuum (concrete) element densities. The design variables are continuous and bounded by ϕ_{min} and ϕ_{max} that in this work are taken as 0 and 1. The volume constraints $c_p(\boldsymbol{\rho})$ are calculated as the sum of the element density ρ_p^e times the element volume v_p^e over all elements e of the considered type ($p = c$ for continuum elements and $p = t$ for truss elements). The allowable amounts of material are the user specified values V_p that herein are taken as $V_t = 365.8$ cm^3 (22.32 in^3) and $V_c = 75\%(L \cdot H \cdot t)$. Throughout the optimization the structure must fulfill the discretized stress-dependent static equilibrium where $\mathbf{K}(\boldsymbol{\rho}_c, \boldsymbol{\rho}_t, \boldsymbol{\sigma}_c, \boldsymbol{\sigma}_t)$ is the global stiffness matrix, $\mathbf{F}$ is the global load vector and $\mathbf{d}$ contains the free displacements.

The truss elements are arranged in a ground structure and allowed to have variable size. The ground structure is placed such that a cover layer is present on the top and bottom of the design domain. For the continuum elements, this work uses the Heaviside projection method [11] as the filtering approach and the Solid Isotropic Material with Penalization (SIMP) [12] method is used to penalize the stiffness of intermediate densities.

In the current work, the Young's moduli of steel and concrete have been taken as $E_c = 25$ GPa (3600 ksi) and $E_s = 200$ GPa (29,000 ksi), respectively. The Poisson's ratio of the concrete is assumed to be $\nu_c = 0.20$.

In Fig 2a the initial design is shown, where the intermediate density concrete elements are grey and the truss elements in the red ground structure are sized equally. Figure 2b gives the final design obtained by solving Eq. (1) with the Method of Moving Asymptotes (MMA) [13] as the gradient-based optimizer. The final design is seen to have a clear black and white description of the force flow in the concrete. Additionally, the reinforcing bars have been sized and reveals a layout with several different sizes in the bottom region of the beam.

2   Digital Fabrication

Three beam types are digitally fabricated, experimentally tested and compared; (i) the standard strut-and-tie design, (ii) the topology-optimized design with prismatic concrete (100% concrete), and (iii) the topology-optimized design with reduced concrete volume (75% concrete). The three designs are shown in Fig.

(a)

(b)
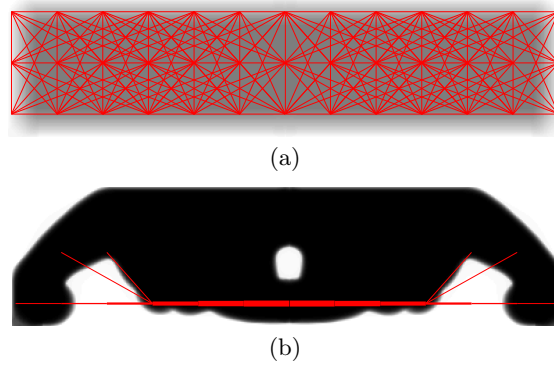
Fig. 2. (a) Initial and (b) final topology-optimized beam designs.

3 where the white volumes show the concrete phases and the hatched regions indicates where reinforcement is placed. Two test specimens are made of each design.

The steel reinforcement is manufactured by sending the digital reinforcement designs to a OMAX CNC-controlled waterjet cutting machine. In this work, the


(a)

(b)

(c)
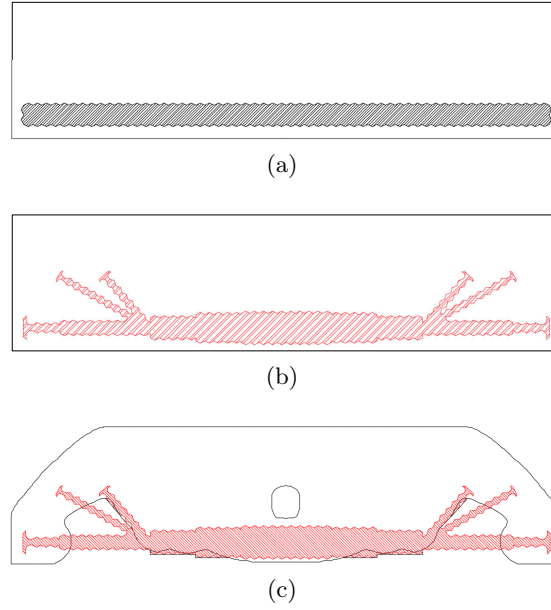
Fig. 3. Experimentally tested designs; (a) standard strut-and-tie design, (b) topology-optimized design with prismatic concrete (100% concrete), and (c) topology-optimized design with reduced concrete volume (75% concrete)

(a)

(b)
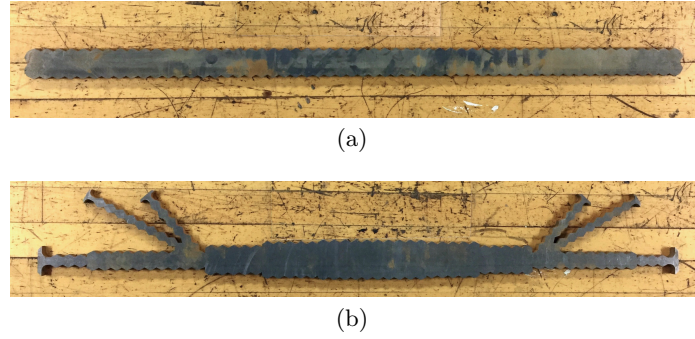
Fig. 4. Examples of waterjet cut steel reinforcement used in beam specimens with (a) standard strut-and-tie design, and (b) topology-optimized designs with both 100% and 75% concrete volumes.

reinforcement is cut from 1.3 cm (0.5") thick steel plates. To improve the bond between concrete and reinforcement, corrugations and anchors are added to the digital layouts. Triangular corrugations are applied to all straight edges and the anchors used in [9] are placed at free ends of the topology-optimized specimens. Figure 4 shows examples of the fabricated reinforcement.

(a)

(b)
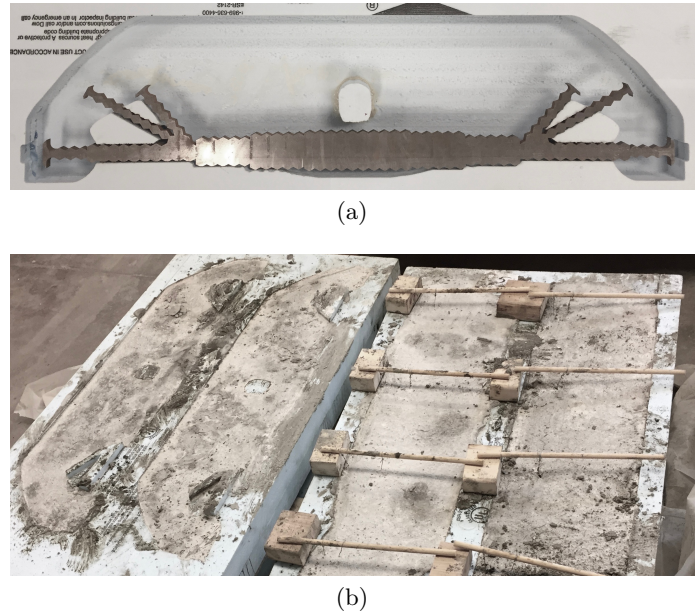
Fig. 5. Concrete casting process where (a) shows a styrofoam mold used for fabrication of a topology-optimized specimen with 75% concrete, and (b) shows the concrete filled molds.

(a)

(b)
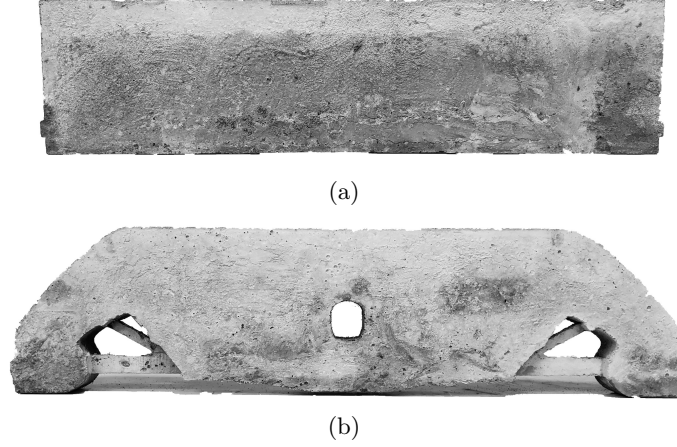
Fig. 6. Examples of digitally fabricated test specimens where (a) is a topology-optimized beam with 100% concrete volume, and (b) is a topology-optimized beam with 75% concrete volume.

The concrete molds are digitally manufactured by CNC milling of styrofoam with an ONSRUD 3-axis mill. The molds are subsequently generously lined with petroleum jelly. A concrete mix is designed with a compressive strength of 27.6 MPa (4 ksi) and poured into the molds. To limit imperfections caused by reinforcement placement, the steel layouts are hanged using wires and wooden dowels. Figure 5 gives an example of a styrofoam mold and shows the casting process.

All test specimens are demolded after two days and placed in a wet environment to hydrate for another 26 days prior to testing. In Fig. 6 examples of the fabricated test specimens are shown.

3 Experimental Results

All specimens are experimentally tested on a Baldwin Universal Testing Machine (UTM). Concrete cylinder tests are first performed to evaluate the quality of the cast concrete. The compressive strengths are found to be reasonably close to the assumed 27.6 MPa (4 ksi) with a variation of -1.8–3%.

For the beam tests, a simulated pin and roller is placed at each end of the considered specimen and a point load is applied at mid-span using displacement control. Figure 7 shows a beam specimen is the testing machine. The beams are loaded until failure is detected the and applied load and resulting deformation is recorded.

Figure 8 gives the results of the experimental investigation. Figure 8a compares the measured mid-point deflections on the x-axis against the applied load on the y-axis. The black dashed line indicates the design load. For the tested

Fig. 7. Experimental set-up used for testing of all beam specimens.

beam specimens in this work, there is seen to be little variation between specimens of the same design. Additionally, brittle failure is observed for all beams without prominent display of ductility or steel yielding. All beams in this work are seen to fail significantly below the design load of $P = 88.9$ kN (20 kips) as the observed maximum loads are in the range 26.7–40.0 kN (6–9 kips). The observed failure modes were consistent for specimens of the same beam type and are shown in Fig. 9.

Upon investigation of the failed beam specimens, it is evident that a pronounced lack of bonding between the concrete and reinforcing steel plates is present. It is easily seen that the steel completely detaches from the concrete,
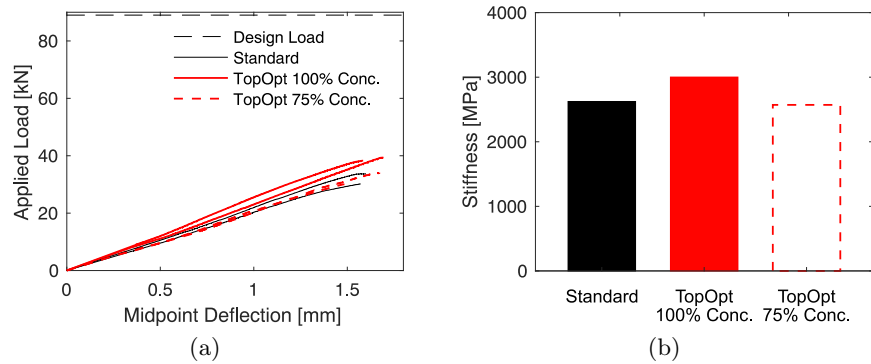

Fig. 8. Experimentally obtained results; (a) load-displacement relations for tested specimens, and (b) average stiffness at $P = 20$ kN (4.5 kips) for each of the design types.

(a)

(b)

(c)
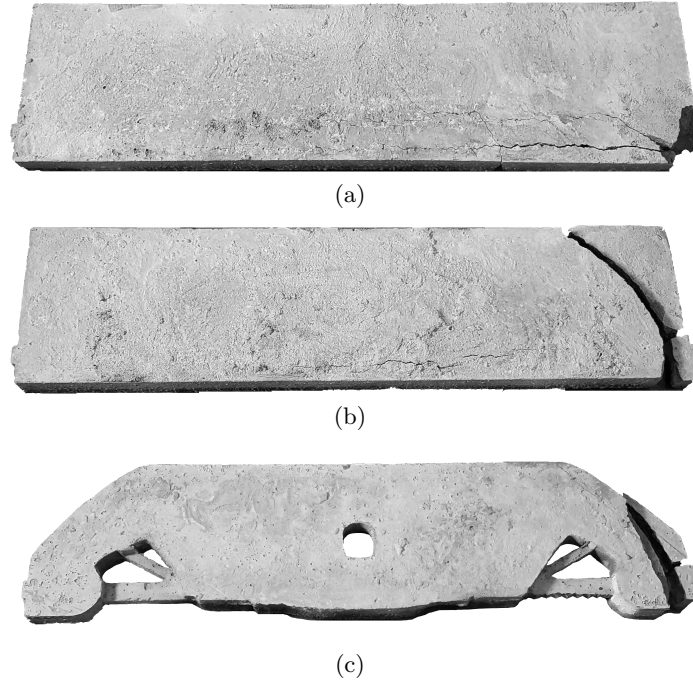
Fig. 9. Beam failures observed for (a) the standard beams, (b) the topology-optimized beams with 100% concrete volume, and (c) the topology-optimized beams with 75% concrete volume.

leaving a polished surface between the two phases. Figure 10a displays an example of the polished surface of the steel and the easily visible gap between concrete and reinforcement. This poor bond quality was observed for all beam specimens in the current work. The poor bond quality is surprising since it was not observed by Jewett and Carstensen [9]. The same reinforcement method was used, however a slightly differently corrugation geometry was applied herein. The corrugations in [9] is shown in Fig. 10b that illustrates the bonding of concrete and reinforcement inside a failed test specimen. This significant difference in bond quality indicates that the corrugation pattern is extremely important for steel-concrete interface along the waterjet cut edges and calls for more research.

Despite the premature failures due to improper concrete-reinforcement bonding, the results in Fig. 8 does suggest some interesting trends about the comparison of the early elastic behaviors of the three beam designs. Figure 8b therefore compares the average stiffness of the three design types at a load of $P = 20$ kN (4.5 kips). As can be seen, the topology-optimized design with 100% concrete has a higher elastic stiffness than the standard strut-and-tie design. This concurs with the conclusions in [9] and is to be expected since the objective of the herein conducted topology optimization is maximize the beam stiffness.
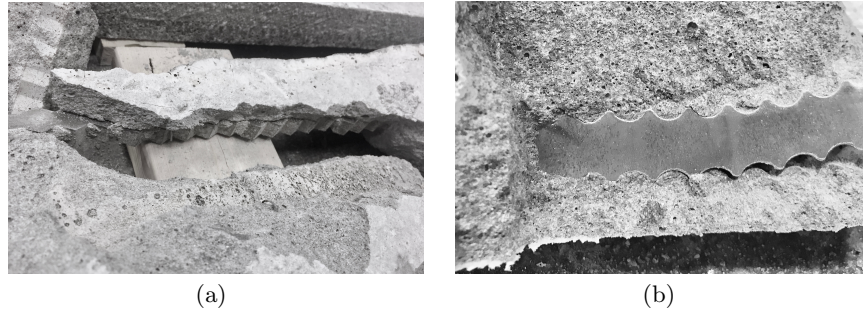
Fig. 10. Concrete-reinforcement after test from (a) the experiments in the current work, and (b) the experiments in [9].

Not surprisingly, performance is lost when removing 25% of the concrete volume. The topology-optimized design with 75% concrete is seen to have a lower stiffness than the topology-optimized beams with 100% concrete. However, it is interesting to note that for the herein considered design case, the experimental behaviors of the standard strut-and-tie beams are nearly identical to the observed performance of the topology-optimized beams with 75% volume. Although more experimental testing is needed to rigorously support this notion, this trend indicates that significant amounts of concrete can be reduced for RC structures if topology optimization is used for the design and fabrication is done by high precision digital construction.

4   Conclusion

This work has used topology optimization as the generative design method for an experimental investigation of digitally manufactured deep RC beams. Three beam design were evaluated where one had a reduced concrete volume. In the early elastic range, the standard design and the topology-optimized beams with reduced concrete exhibited near identical behaviors. This might indicate that low weight RC design with similar properties as conventionally designed structures can be achieved.

To improve precision of the produced reinforcement, steel plates were cut by waterjet. However, in the current work, a poor bond quality of the concrete and reinforcement was obtained. This prevented a complete comparison of the tested specimens. More experimental testing is therefore needed to underbuilt the performance comparisons made in this work, and to rigorously investigate if the governing failure modes are different from those observed in conventional RC design. Additionally, more investigation of corrugation patterns is recommended if steel plates are to be used as reinforcement in future studies.

References

1. Bendsøe, M.P., Sigmund, O.: Topology optimization: Theory, methods and applications. 1st edn. Springer-Verlag, Berlin (2003)
2. Liang, Q.Q., Xie, Y.M., Steven, G.P.: Topology optimization of strut-and-tie models in RC structures using an evolutionary procedure. Structural Journal, **97**(2), 211–330 (2000)
3. Gaynor, A., Guest, J.K., Moen, C.D.: RC force visualization and design using bilinear truss-continuum topology optimization. Journal of Structural Engineering **139**(4), 607–618 (2012)
4. Amir, O., Shakour, E.: Simultaneous shape and topology optimization of prestressed concrete beams. Structural and Multidisciplinary Optimization, **57**(5), 1831–1843 (2018)
5. Pastore, T., Mercuri, V., Menna, C., Asprone, D., Festa, P., Auricchio, F.: Topology optimization of stress-constrained structural elements using risk-factor approach. Computers & Structures, **224**, 106104 (2019)
6. Dombernowsky, P., Søndergaard, A.: Design, analysis and realisation of topology optimized concrete structures. Journal of the International Association for Shell and Spatial Structures **54**(4), 209–216 (2012)
7. Jipa, A., Bernhard, M., Dillenburger, B., Meibodi, M.: 3D-printed stay-in-place formwork for topologically optimized concrete slabs. In: 2016 TxA Emerging Design+Technology Conference Proceedings, pp. 97–107. Texas Society of Architects, San Antonio, TX (2016)
8. Jewett, J.L., Carstensen, J.V.: Topology-optimized design, construction and experimental evaluation of concrete beams. Automation in Construction **102**, 59–67 (2019)
9. Jewett, J.L., Carstensen, J.V.: Experimental investigation of strut-and-tie layouts in deep RC beams designed with hybrid bi-linear topology optimization. Engineering Structures **197**, 109322 (2019)
10. ACI. Building code requirements for structural concrete (ACI 318-08) and commentary. American Concrete Institute, (2008)
11. Guest, J. K., Prévost, J. H., Belytschko, T. Achieving minimum length scale in topology optimization using nodal design variables and projection functions. International Journal of Numerical Methods in Engineering **61**(2), 238–254 (2004)
12. Bendsøe, M. P. Optimal shape design as a material distribution problem. Structural Optimization **1**(4), 193–202 (1989)
13. Svanberg, K.: The method of moving asymptotes: A new method for structural optimization. International Journal of Numerical Methods in Engineering **24**(2), 359–373 (1987)